HHS Public Access

Author manuscript

Biotechnol Prog. Author manuscript; available in PMC 2018 November 28.

Published in final edited form as:

Biotechnol Prog. 2016 May ; 32(3): 745–755. doi:10.1002/btpr.2257.

Development of an Infusion Bioreactor for the Accelerated Preparation of Decellularized Skeletal Muscle Scaffolds

Ben Kasukonis[1], **John Kim**[1], **Tyrone Washington**[2], and **Jeffrey Wolchok**[1]

[1]Department of Biomedical Engineering, College of Engineering, University of Arkansas

[2]Department of Health, Human Performance, and Health Professionals, College of Education and Health Professionals, University of Arkansas

Abstract

The implantation of decellularized tissue has shown effectiveness as a strategy for the treatment of volumetric muscle loss (VML) injuries. The preparation of decellularized tissue typically relies on the diffusion driven removal of cellular debris. For bulky tissues like muscle, the process can be lengthy, which introduces opportunities for both tissue contamination and degradation of key ECM molecules. In this study we report on the accelerated preparation of decellularized skeletal muscle (DSM) scaffolds using a infusion system and examine scaffold performance for the repair of VML injuries. The preparation of DSM scaffolds using infusion was dramatically accelerated. As the infusion rate (1% SDS) was increased from 0.1 to 1 and 10ml/hr, the time needed to remove intracellular myoglobin and actin decreased from a maximum of 140±3hrs to 45±3hrs and 10±2hrs respectively. Although infusion appeared to remove cellular debris more aggressively, it did not significantly decrease the collagen or glycosaminoglycan composition of DSM samples when compared to un-infused controls. Infusion prepared DSM samples retained the aligned network structure and mechanical integrity of control samples. Infusion prepared DSM samples supported the attachment and in-vitro proliferation of myoblast cells and was well tolerated by the host when examined in-vivo.

Keywords

decellularization; extracellular matrix; skeletal muscle; scaffold

1. Introduction

Our group is pursuing the development of biomaterials targeting the repair of damaged skeletal muscle tissue. Skeletal muscle has a strong capacity for repair, yet this capacity can be overwhelmed when damage is severe. Following mild injuries like strains and contusions, in which the myocytes are damaged but the underlying muscle structure and satellite cell population is preserved, regeneration is robust and surgical intervention is not indicated [1, 2].

Corresponding Author: Jeff Wolchok, 125 Engineering Hall, Department of Biomedical Engineering, University of Arkansas, Fayetteville, AR 72701, jwolchok@uark.edu, 479 575-2850.

Author Disclosure Statement:
No competing financial interests exist for any of the authors.

However, when significant muscle volume is lost (trauma or surgical resection) the underlying structure and progenitor cell pool is absent and regeneration is poor. Termed volumetric muscle loss (VML), the bulk loss (>20%) of muscle tissue overwhelms the capacity for repair, leading to the formation of non-contractile scar tissue at the defect site and functional impairment for the patient [3]. The poor outcome following VML injury, motivates the need for a treatment option. A promising approach is restoration of the chemical and physical cues provided by the extracellular matrix (ECM).

To restore these cues, our group is exploring the use of ECM biomaterials derived from skeletal muscle. To improve the isolation of ECM from whole muscle tissue, a new decellularization approach was explored in this study. Commonly, the decellularization of whole tissues employs detergents (ex: sodium dodecyl sulfate) to lyse cell membranes and remove intracellular proteins, followed by DNAse/RNAse rinses to remove residual nucleic acids [4, 5]. The initial removal of intracellular proteins using detergents is typically a diffusion driven process, which for thicker tissues like skeletal muscle can be lengthy, requiring two weeks or more[6]. This introduces opportunities for both tissue contamination and degradation of key ECM molecules. In an effort to accelerate the process, the active delivery of detergents into whole organs has been achieved via vascular perfusion. The major inlets and outlets (arteries and veins) along with capillary networks are utilized to perfuse the entire organ. Perfusion decellularization has been used to produce whole organ scaffolds for the heart [7], liver [8], lungs [9], kidneys [10], and recently even entire limbs [11].

Skeletal muscle tissue lacks the easily accessible major arteries and veins that are found in whole organs, motivating an alternative delivery approach. The common utilization of intramuscular injection would suggest that fluid infusion through skeletal muscle might provide a viable delivery route for decellularization agents. Towards this end, our group has developed a scalable bench top infusion platform that uses a needle rather than the vascular system to deliver detergents deep into muscle tissue with the goal of accelerating the removal of intracellular proteins. The system also explores the distinct color change (red to white) that occurs within skeletal muscle tissue as myoglobin is removed during decellularization as a means to non-invasively monitor the removal of intracellular proteins. The design/fabrication of the device, characterization of its performance, and measurement of infusion prepared decellularized skeletal muscle (DSM) properties are described in this report. Ultimately, we believe these materials could find utility as scaffolds for the repair of VML injuries.

2. Methods

2.1 Absorbance Properties of Skeletal Muscle

A visible light absorbance sweep was performed on rat (Sprague Dawley) gastrocnemius muscle samples in order to characterize the optical properties of whole and decellularized skeletal muscle. The changes in muscle absorbance properties that occur with decellularization would be utilized during the subsequent design of an optical monitoring approach. Rat muscle was selected based on its past use in muscle regeneration animal studies and the anticipated area of application for this device [12]. All whole muscle tissues used in this study were collected from cadaveric animals that had been previously

euthanized using methods approved by the University of Arkansas Institutional Animal Care and Use Committee (IACUC) approved study (protocol #12026). All tissues were stored at −20°C until required for testing. In preparation for testing, gastrocnemius muscle samples were dissected, and from each whole muscle sample a central core was harvested using a biopsy punch (diameter = 6mm) and trimmed to a thickness of 2mm. Cylindrical muscle sample cores were incubated in a 1% sodium dodecyl sulfate (SDS) solution (10mM Tris HCL) with agitation for 24 and 48 hours at room temperature following published protocols[13]. Untreated muscle samples were maintained as controls (n=4 / sample group). At the prescribed time points (24, and 48 hours) muscle core samples were loaded into 96 well plates (one sample per well) and a spectral sweep of tissue absorbance was measured (400–900nm, step size = 5nm) with the aid of a spectrophotometer (Synergy H1, BioTek, Winooski, VT). For comparison, the absorbance of myoglobin, an abundant intracellular skeletal muscle protein, was also characterized (0.1, 0.3, and 0.6% in phosphate buffered saline). Absorbance versus wavelength data for all muscle and myoglobin samples were plotted and examined for the presence of decellularization sensitive absorbance features.

2.2 Infusion Bioreactor Design and Fabrication

The design goal was to combine continuous tissue infusion and real time optical monitoring into a single bench top device. The two primary components of the device are the muscle infusion units and optical detection collars with integrated data collection hardware and software. The infusion units, optical monitoring collars, and data collection hardware are housed within and mounted onto a custom fabricated (Replicator 2, MakerBot Industries, New York City, NY) two-piece enclosure (Figure 1). The enclosure was designed to accommodate four individual infusion units each capable of accommodating a single muscle tissue sample. The closure also isolates the optical monitoring collars from ambient light. Each of the four modular infusion units consists of a rigid acrylic cylinder (ID = 10mm; length = 40mm) that forms a translucent infusion chamber. The inlet and outlet of each chamber is enclosed by watertight ports fashioned with Leur lock style fittings and fabricated in acrylic with the aid of a 3-D printer (Objet 30, Objet, Israel). The inlet port incorporates a removable 26-ga stainless steel hypodermic needle (length = 20 mm). The needle is used to deliver solution into the interior of individual whole muscle samples. The flow of fluid into each infusion unit was controlled via a commercial multi-syringe pump (#552219, Harvard Apparatus, Holliston, MA) capable of delivering fluid to all four chambers over the range of flow rates (0.1 to 10ml/hr) that would be evaluated during device characterization. Waste decellularization solution is collected in a reservoir for disposal or evaluation.

The optical collar was fitted with a single light emitting diode (LED) producing a peak emittance centered at 535nm. Peak LED wavelength selection was motivated by the results of the previously described muscle optical property characterization. The light output of the LED is directed across the diameter of the optical collar. A light detecting resistor (LDR) was positioned opposite to the LED. The LDR converts light intensity in photons to resistance in ohms. The optical collar with integrated LED and LDR can be positioned along the length of the infusion unit. During infusion, the collar is positioned over the muscle sample, such that muscle tissue impedes the light path from the LED emitter to the LDR

detector. Analog voltages collected from the LDR were converted to digital values using an 8-bit analog-to-digital converter (ADC) (Adafruit Industries, New York, NY). A miniaturized single board computer (Raspberry Pi Foundation, United Kingdom) was used to power the LEDs and to control collection of the digitized LDR voltage signal from the ADC. Custom designed software (Python) was created to collect the voltage data and log it to an online spreadsheet. Optical data was collected from the LDR every five minutes. The complete system, including syringe pump and flat screen monitor, occupies a 0.5m X 0.5m footprint, a space that is compatible with typical laboratory workbenches.

2.3 Bioreactor Characterization

For all device characterization testing, medial gastrocnemius muscle tissue was harvested from cadaveric Sprague Dawley rats and stored at −20°C until needed for testing. Prior to testing all muscles were thawed and rinsed briefly in DI water to remove any superficial blood or loosely adhered tissue. Whole muscle samples were loaded into infusion chambers, one muscle per chamber. The position of the muscle was adjusted until the needle tip was located at the mid-belly (thickest) region of the muscle. Based on static decellularization pilot testing and guided by published methods [13], muscle samples (n=4) were infused using a 1% SDS solution at a flow rate of 1ml/hr while LDR output was recorded and plotted. Samples were collected when muscle optical properties (LDR output) were unchanged (<0.1% difference from the previous recording) for five continuous recordings (25 minutes).

To examine the effectiveness of infusion treatment as a method for intracellular protein removal, representative infusion treated and untreated whole muscle samples were embedded in tissue freezing media (Triangle Biomedical Sciences, Durham, NC), sectioned at 8μm with a cryostat, and mounted onto glass microscope slides. Mounted sections were immune-reacted for the presence of myoglobin (rabbit IgG_1, 1:500, Sigma, St. Louis, MO) and actin (phalloidin, 1:40, Sigma, St. Louis, MO) followed by incubation with the appropriate fluorescently labeled secondary antibodies (Alexafluor, 1:500, Fisher Scientific). Sections were counterstained with the nuclear staining reagent DAPI, and then microscopically imaged (Ci-L, Nikon, Troy, NY). Digital images were captured, stored, and examined for the presence of intracellular proteins and nuclear remnants.

To explore the influence of key infusion parameters (flow rate and SDS solution concentration) on myoglobin removal, medical gastrocnemius muscle samples were perfused at flow rates of either 0.1, 1, or 10ml/hr using SDS solutions at concentrations of 0.2% or 1%. A total of 6 parameter combinations were explored (n= 4/ parameter condition). Throughout infusion testing the optical properties of each muscle was measured and digitally logged every 5 minutes. As previously described, the time at which intracellular protein removal was considered complete and samples were removed was recorded as the time at which sample optical properties were unchanged for five continuous recording.

From the infusion data, the time to reach steady state optical properties (y) was modeled with a two factor (1: flow rate, 2: SDS concentration) regression model of the type

$$y = b_0 + b_1x_1 + b_2x_2 + b_{12}x_1x_2 \quad (1)$$

The regression coefficients (b_i) were solved for using commercially available data analysis software (JMP, SAS Institute, Cary, NC). From the model, the relationship of infusion time to each of the infusion parameters was calculated.

To determine whether infusion influenced the retention of key ECM molecules, the sulfated glycosaminoglycans (sGAG) concentration was quantified using a published procedure[14]. For comparison, control DSM samples were statically (non-infused) incubated in 1% SDS at room temperature with gentile agitation using rocker platform, for a duration of two weeks [6]. All infusion and control samples were lyophilized and stored at −20°C until needed for analysis. To extract sGAG. lyophilized samples (n=4/sample group) were digested in a solution containing 50 μg/mL proteinase K in 100 mM K_2HPO_4 at a pH of 8.0 at 55ºC for 16 hours. The samples were then centrifuged and filtered to isolate tissue fragments. A 1,9-dimethylmethylene blue (DMMB) solution was added to produce an insoluble GAG-DMMB complex. The solution was centrifuged, the supernatant was removed, and the GAG-DMMB complex was dissolved with a decomplexation solution. The absorbance of the resulting solution was read at 656 nm with the aid of a microplate reader (Synergy H1, BioTek, Winooski, VT). Samples were tested in triplicate and compared against a standard curve to determine sGAG concentration.

The collagen content of control and infusion samples (n=4/sample group) was quantified using a modified version of the hydroxyproline assay procedure reported by Edwards [15]. Briefly, all tissue samples were hydrolyzed in 6N HCl for 16–20 hours at 115ºC, then cooled to room temperature and diluted 1:5 in distilled water. Hydrolyzed samples were mixed with a chloramine T solution (1:2) and incubated at room temperature for 20 minutes. A dimethylaminobenzaldehyde assay solution was added (1:2) and the mixture was incubated at 60°C for 15 minutes to develop a red chromophore. Sample absorbance was read at 570 nm using a microplate reader. Samples were tested in triplicate and compared against a standard curve to determine collagen concentration. To visualize and validate the retention of collagen within infusion prepared tissue, a representative sample was immunoreacted for the presence of collagen type I (mouse IgG_1, 1:500, Sigma, St. Louis, MO) and type III (rabbit IgG_1, 1:1000, AbCam, UK) followed by incubation with the appropriate fluorescently labeled secondary antibodies (Alexafluor, 1:500, Fisher Scientific).

To explore the influence of infusion treatment on DSM physical properties, control and infusion (1% SDS for 12 hours at 10ml/hr) DSM sample (n=4/sample group) mechanical properties were measured with the aid of a uni-axial tensile tester (UStretch, CellScale, Ontario, Canada) using techniques familiar to our group [16–18]. Hydrated (PBS, pH=7.4) sample strips (12 mm X 3 mm) were deformed at a constant strain rate of 1%/s until failure using a 5N load cell while the load and displacement values were recorded. For each sample, engineering stress versus strain curves were generated from load and elongation data. Strain was determined using grip displacement values. From each curve the tangent modulus was calculated from a linear fit to the stress-strain curve. The ultimate strength was calculated as the peak stress achieved by each sample prior to failure.

Additional control and infusion prepared DSM samples (n=4/sample groups) were embedded in tissue freezing medium and sectioned transversely (8um) with the aid of a

cryostat. Sections were mounted onto glass slides, stained with hematoxylin and eosin (H&E) and microscopically imaged (100x). Three representative images from each sample were used to measure porosity (% open space) and network alignment (average orientation angle) using image analysis software (ImageJ) and guided by published techniques [19, 20]. For DSM sample orientation analysis, the direction of muscle contraction (long axis of the gastrocnemius muscle) was selected to correspond to an orientation angle of 0 degrees.

2.4 In-Vitro and in-Vivo Biocompatibility

To create DSM samples for implantation, Sprague Dawley tibialis anterior (TA) muscle was infusion treated (1% SDS for 12 hours at 10ml/hr) using the previously described and characterized system. Following infusion treatment, samples were statically incubated overnight in a DNAse / RNAse solution (1kU/ml DNAse in a 10mM Tris-HCL buffer; 2.5mM $MgCL_2$ + 0.5mM $CaCl_2$) and then incubated (8 hours) in a 1X penicillin/ streptomycin solution to reduce the risk of infection. Samples were rinsed thoroughly (a total of six 24 hour wash steps) in PBS following each preparation step (Figure 2). Following completion of the entire decellularization protocol, the DNA concentration of representative DSM implants (n=3) was measured with the aid of a commercial quantification kit (Qubit, Fisher Scientific). DSM implants were lyophilized and stored at −20C until needed for implantation.

A direct contact assay was used to evaluate cellular attachment and proliferation upon infusion prepared DSM substrates. DSM material islands (diameter = 6mm) were created on glass microscope slides. DSM islands were seeded with skeletal muscle myoblasts (L6, ATCC, Manassas, VA) at a density of 7K cells per island. Cell viability was evaluated at 3 and 7 days (n= 3 islands / time point) using calcein AM (Life Technologies). Three representative fields were imaged (100x) from each island and captured digitally. From the digital images, cell confluency (% surface coverage) was calculated at each time point with the aid of image analysis software (ImageJ).

In-vivo host response was examined using a dorsal subcutaneous implant site. *In-vivo* biocompatibility was assayed at short-term (4 weeks) and long-term (12 weeks) time points. Mature male Sprague Dawley rats (300+g) were used (Harlan, IN). All surgical procedures were performed in accordance with protocols approved by the University of Arkansas Institutional Animal Care and Use Committee. Anesthesia was induced using isoflurane (2–4%) in oxygen. The subcutaneous implant site was surgically exposed through a 2 cm left-right incision placed 2 finger widths caudal to the scapulae. A subcutaneous pouch was created in each animal by blunt dissection. A single perfusion prepared DSM disk (6mm diameter X 1mm thick) was implanted into each pouch (Incisions were closed using surgical adhesive (VetBond, 3M). Following surgery all animals were housed in the University of Arkansas Central Laboratory Animal Facility. At the prescribed time-points (4 and 12 weeks) all animals (n=3 / timepoint) were euthanized via inhalation of carbon dioxide. The implant site with surrounding soft tissue was harvested, fixed in 4% paraformaldehyde, paraffin embedded, sectioned (10um), and stained with H&E with the aid of the University of Arkansas Histological Core Facility. Stained sections were imaged and examined for evidence of material degradation.

3. Statistics

All data is represented by the mean and standard deviation Comparisons between infusion flow rate and SDS concentration (time to stable optical properties, collagen, and sGAG analysis) were evaluated with a two-factor ANOVA. Post hoc comparisons were made using Tukey's test. The effect of treatment (infusion version control) on alignment, porosity, and mechanical properties was evaluated using a two-way student's t-test. A standard 0.05 level of significance was used for all statistical tests.

4. Results

4.1 Absorbance Properties of Skeletal Muscle

The absorbance sweeps collected from myoglobin solution samples (0.6%) were characterized by an observable peak centered at 505±4nm (Figure 2). As the myoglobin concentration was decreased to 0.3% and 0.1%, the absorbance peak heights decreased by 58% and 85% respectively and the peak profiles tended to broaden. The absorbance sweeps recorded from hydrated whole muscle samples were characterized by a more modest absorbance shoulder, which when compared to myoglobin was less pronounced and shifted modestly towards a higher wavelength (541±7nm). The whole muscle peak wavelength was positioned within the green region of the visible light spectrum. Following 24 hours of SDS incubation, the absorbance shoulder was still detectable but less pronounced. Visually, 24 hour muscle samples showed residual evidence of intracellular myoglobin (retention of a pinkish color), suggesting partial but still incomplete removal. After 48 hours of SDS treatment, the absorbance shoulder present in whole muscle samples was no longer detected and myoglobin was no longer visualized, as evidenced by a translucent appearance. Generally, the absorbance of skeletal muscle tissue at 541nm decreased as samples were progressively incubated in SDS, suggesting a valuable target wavelength for optical monitoring of intracellular myoglobin retention.

4.2 Bioreactor Characterization

Muscle sample absorbance logs (LDR voltage versus time) were characterized by a progressive reduction in tissue absorbance (decreased LDR output voltage) with increased infusion time as more light (535nm) emitted by the LED was capable of transmitting through the muscle samples and reaching the LDR. Whole muscle samples transitioned from a characteristic red color to translucent during the infusion driven removal of intracellular proteins. (Figure 3). LDR voltage eventually reached a steady state minimum for all samples tested, which was defined for all subsequent tests as the time to myoglobin removal. Prior to infusion treatment, intracellular myoglobin, as well as actin and nuclear remnants where visible within whole muscle sections. Once the LDR had reached a steady minimum, identified as the time at which LDR output voltage was unchanged for 25 minutes, infusion treated muscle samples (n=4) were no longer immunoreactive to myoglobin or actin. Furthermore, although not treated with nucleases during the infusion process, DAPI positive nuclei could not be detected. Overall, the histological examination of infusion treated samples suggests that the LDR voltage minimum was an effective metric of intracellular myoglobin and actin removal.

The infusion solution flow rate and SDS concentration had a statistically significant effect on the removal of intracellular myoglobin (Figure 4). The average infusion time required to remove myoglobin, as measured by LDR voltage and further validated through histology, was shortened in response to increases to both flow rate and SDS concentration. Flow rate had a strong influence on myoglobin removal. The removal time decreased from a maximum of 143±8hrs at the lowest flow rate of 0.1 ml/hr (0.2%SDS) to 42±3hrs and 9±1hr as the flow rate was increased to 1ml/hour and 10ml/hour respectively. Increased SDS concentration had a significant but less dramatic influence when compared to flow rate. Increasing the SDS concentration from 0.2% to 1% shortened the time from 143±8hrs to 107±6 at the lowest flow rate tested (0.1ml/hr), a reduction of 24%. At higher flow rates (1 and 10ml/hr) the effect of SDS concentration on myoglobin removal was less pronounced, but still statistically significant. When viewed as a whole, the removal of intracellular myoglobin was more responsive to flow rate than SDS concentration, however the range of flow rates tested (100 fold difference between lowest and highest) was larger than the range of SDS concentrations tested (5 fold difference). From the data collected, the relationship of myoglobin removal time (in hours) to flow rate (ml/hr) and SDS concentration (%) was modeled (eq. 2). When plotted over the parameter ranges tested (Figure 4B & C), the model accurately describes the increased influence of flow rate on myoglobin removal time observed during benchtop testing.

$$\text{Time} = 99 - 8.3 \times [\text{Flow}] - 18.0 \times [\text{SDS}] + 2.7 \times (\text{Flow} - 0.6) \times (\text{SDS} - 3.7) \quad (2)$$

Although SDS infusion accelerated the removal of intracellular myoglobin and actin, it did not significantly decrease collagen or sGAG concentration when compared to non-infused controls. No statistically significant differences in collagen or sGAG concentration were detected for any of the flow rates and SDS concentrations examined (Figure 5). All infusion treated collagen and GAG composition values were within 10% of control samples. Furthermore, trends indicating a relationship between ECM composition and infusion flow rate were not observed.

Infusion decellularized samples retained the highly aligned network organization characteristic of skeletal muscle (Figure 6). The dominant orientation angle of DSM samples following infusion decellularization (7±6°) was not significantly different from controls (11±5°). Both infusion prepared and control samples were aligned in the direction of contraction (designated as 0°). Control and infusion prepared samples were robust and easily tolerated handling and tensile testing. Stress versus strain curves for both materials were characterized by in initial toe-in region out to approximately 10–15% strain followed by a nearly linear (R^2>0.9) increase is stress extending out to failure at approximately 100–125% for both infusion and control DSM samples. The average tangent modulus measured from the linear region extending from 20% (post toe-in) to material failure was 225±44kPa and 189±32kPa for infusion and control samples respectively. Average infusion prepared DSM sample elastic moduli was not significantly different from control samples. Similarly, average ultimate strength differences between infusion and control DSM materials were not statistically significant.

4.3 In-Vitro and in-Vivo Biocompatibility

Average infusion prepared DSM sample DNA content (2.9±0.6ng of DNA / mg of tissue) were well below the preferred implantation threshold (< 50–70ng/mg) reported by others [21, 22]. The DSM samples supported the attachment and *in-vitro* proliferation of cultured myoblast cells. Viable cells were attached to all cell seeded DSM islands at both time points. Seventy-two hours after seeding, viable cells covered, on average, 8±2% of the DSM sample surface (Figure 7). By seven days post seeding, average cell coverage increased to 60±6% of the DSM sample surface. Cells cultured on DSM materials appeared well spread and expanded upon the DSM surface at a coverage rate of approximately 13% / day. The average cell coverage difference between day three and seven was statistically significant.

All implanted animals tolerated the subcutaneous implantation surgery well and reached the prescribed study endpoints without complications (n=4 / endpoint). At four weeks post implantation, DSM materials were well incorporated into the surrounding tissue and host cells had densely penetrated the material (Figure 8). While signs of active inflammation could be observed there were no signs of tissue necrosis or exudate (pus) accumulation at the implant site. The dense cellular penetration into the DSM material was suggestive of active remodeling of the implant site. The breakdown of whole DSM disks into smaller fragments was observed. There were no signs suggesting formation of a dense fibrous encapsulation layer surrounding DSM materials. By twelve weeks post implantation, DSM materials appeared fully degraded. No evidence of DSM material could be identified in any of the implanted animals, although some residual cellularity could be seen at the implant site.

5. Discussion

As chemical decellularization schemes continue to mature and gain acceptance, the development of effective delivery platforms deserves research investment. With that goal in mind, what was explored in this study is a device and method for the preparation of decellularized skeletal muscle tissue using a non-vascular infusion delivery method. Overall, the utilization of infusion on skeletal muscle samples was highly effective at accelerating the removal of intracellular proteins. Specifically, with the aid of the infusion device, the time to clear rat lower limb gastrocnemius and TA muscles of intracellular proteins reduced from two weeks to a short as 10 hours. This is a notable finding, and the first we are aware of that demonstrated the accelerated removal of cellular debris from bulk tissue samples using a nonvascular infusion technique. It may be possible to translate this process to other tissues, particularly musculoskeletal tissues including, tendons [23], ligaments [24], cartilage [25], and menisci [26] in which vascular perfusion would be difficult. The time reduction is not just important from the standpoint of process efficiency, but also may help reduce the degradation of key ECM proteins that could occur with time throughout the decellularization process. The decellularization of tissue using SDS, the most common process, is typically performed at room temperature, and while the presence of SDS limits bacterial and fungal growth, the degradation of proteins that can occurs with time at room temperature is a concern [27, 28]. Shortening the amount of time tissue is exposed to room temperatures in

aqueous solutions may reduce the degradation of key ECM proteins during decellularization and improve scaffold quality.

While the device described in this study was designed for the processing of small animal tissues for use in pre-clinical research, the future application of infusion to accelerate the preparation of human or large animal tissue for clinical applications is anticipated. Particularly since the complete removal of cellular debris from large skeletal muscle tissues, like the quadriceps which can be several centimeters thick, may be prohibitively lengthy using diffusion alone. It should also be noted that human skeletal muscle tissue is rarely if ever tissue banked, and therefore represents an untapped source for implantable human ECM. Device scale-up for the processing of larger muscle tissue will require design adaptations beyond just increasing the size of the chambers. The single needle infusion chambers developed in this study were designed for the processing of single rat hind limb skeletal muscles. The volume of rat gastrocnemius and tibialis anterior muscles (1–2 cm^3) was well suited to the delivery of decellularization solution via a single hypodermic needle. However, the processing of larger animal and potentially cadaveric human muscle samples for clinical applications would require modification to incorporate a multi-needle approach. While clearly more complex, our experience with the current single needle system suggests that expansion to a multi-needle system is achievable, and in fact the current system uses multiple needles to process muscle samples in parallel. What remains unknown, is the optimal relationship between needle quantity, spacing, and tissue volume. Future bench top measurement and computer modeling of the relationship between time to decellularization and tissue volume would help determine ideal infusion needle density.

It should be possible to utilize lower SDS concentrations than those explored in this study, while still maintaining overnight to at most 1 day myoglobin removal times. At an infusion flow rate of 10ml/hr, the highest rate tested, a 5 fold decrease in SDS concentration (0.2% versus 1%) only increased the time from 7 to 9 hours suggesting an even lower SDS concentration might still be effective. A reduction in SDS concentration could be beneficial when one considers that removing SDS from tissue is challenging and the presence of residual SDS within implanted scaffolds can be cytotoxic [29]. Furthermore, it is well established that exposure to SDS during the decellularization process can have a detrimental effect on tissue properties [30]. Eventually it may be beneficial to transition towards SDS-free decellularization approaches. If so, it seems reasonable to suggest that infusion could be utilized to decrease process duration for other solution based decellularization strategies, including SDS-free techniques that employ osmotic or physical means to disrupt cell membranes and liberate intracellular debris [31, 32]. Alternatively, it may be possible to utilize a short SDS incubation step to initially lyse cells and bind intracellular proteins, followed by a longer SDS-free infusion step to wash away the intracellular debris and residual SDS. Whatever the method, it should be possible to utilize infusion as a means to minimize both the SDS concentration and exposure time during the decellularization process.

The monitoring of skeletal muscle optical properties provided a non-destructive real time means to evaluate decellularization progression. The histological results from this study suggest that the monitoring of muscle optical properties is a good indicator of intracellular myoglobin concentration. While we only looked at one additional intracellular protein

(actin) it seems reasonable to speculate that if these two proteins were effectively removed other intracellular proteins were as well. One limitation is that optical monitoring of the type used the current device was designed to detect the progressive removal of the muscle specific intracellular protein myoglobin. The progressive removal of myoglobin produced an obvious shift in tissue appearance from red to clear, which could be detected in the visible region of the light spectrum using a low cost LED and LDR pairing. However, it has been suggested that removal of the nuclear debris is more crucial to implant performance than the intracellular proteins, suggesting that development of a means to monitor the removal DNA and RNA would be valuable [5]. Unfortunately, the optical properties of muscle within the visible region are not affected by the removal of nuclear debris. As an adjunct to the currently monitoring approach, it may be possible to examine the optical properties of tissues at DNA/RNA sensitive wavelengths (260/280nm) to monitor the removal of nuclear debris, although using low cost LEDs to do so is not feasible.

The co-delivery of muscle progenitor (satellite) cells in combination with ECM could also help stimulate a pro-regenerative environment following VML injury. The loss of muscle tissue following VML eliminates a substantial pool of progenitor cells. The remaining satellite cell population available for migration from surrounding healthy tissue may be inadequate, and therefore supplementation of the repair site with additional progenitor cells could enhance regeneration. Towards this end, the in-vitro seeding of ECM implants with progenitor cells has been shown to improve the restoration of peak contractile force [6, 33]. With this approach in mind, infusion flow could be used as a means to seed DSM implants with progenitor cells in preparation for implantation. Infusion could help distribute cells evenly throughout the DSM network, rather than densely at the surface as is generally observed following manual seeding[34]. Satellite cells are difficult to amass in great quantities, and can lose their regenerative capacity when expanded *in vitro* [35] so improving the efficiency of in-vitro progenitor cell delivery has value.

The average DSM modulus values measured in this study are similar in magnitude to other decellularized tissue scaffolds, including commercially available porcine intestinal and bladder tissue [36, 37], as well as human facial DSM material [38]. The relationship between scaffold modulus and VML repair outcome has not been investigated, but invitro studies have shown that muscle progenitor cells sense and respond to substrate stiffness. Muscle progenitor cell myogenesis is significantly enhanced when the cells are grown on soft substrates like ECM and reduced on stiff substrates like tissue culture plastic [39, 40]. Similar cell-substrate stiffness interactions have been noted for other cell types including cardiomyocytes [41]. Furthermore, the robust mechanical properties of DSM and other ECM scaffolds facilitate attachment (suturing) to the surrounding healthy tissue during surgical VML repair. Surgical reattachment is clinically important, because it will enable the transfer of contractile force through the repair site during healing and regeneration. This is potentially critical, since force and substrate strain have been shown to enhance muscle progenitor cell myogenesis [42, 43].

While the ideal VML repair scheme still awaits discovery, it appears the restoration of a pro-myogenic environment may require a multifactorial approach, combining biocompatible scaffolds, with progenitor cells, soluble myogenic signaling molecules, and postoperative

rehabilitation [44, 45]. The accelerated removal of intracellular proteins from skeletal muscle tissues, without sacrificing chemical or physical properties, makes the infusion preparation platform described in this study an attractive scaffold preparation strategy. Furthermore pilot study biocompatibility testing suggesting that infusion prepared DSM both supported cell attachment and was well tolerated by the host, motivates further *in-vivo* examination using a peer accepted muscle regeneration animal model [46].

6. Conclusions

The key findings of this study suggest that:

1) The delivery of SDS into skeletal muscle via infusion removed intracellular proteins including myoglobin and actin.

2) The monitoring of myoglobin absorbance was effective as an inexpensive means to noninvasively monitor the progression of intracellular protein removal during decellularization.

3) Infusion flow rate and SDS concentration could be adjusted to modulate the removal rate of intracellular proteins from whole muscle samples.

4) Infusion did not reduce the collagen or sGAG composition of DSM scaffolds.

5) Infusion did not influence the native network alignment or reduce the mechanical properties of DSM scaffolds.

6) Infusion prepared material supported the attachment and proliferation of cells and was well tolerated by the host following subcutaneous implantation.

Acknowledgments:

Research reported in this publication was supported by the National Institute Of Arthritis And Musculoskeletal And Skin Diseases of the National Institutes of Health under Award Number R15AR064481 and the Arkansas Biosciences Institute.

References

1. Hill M; Wernig A; Goldspink G, Muscle satellite (stem) cell activation during local tissue injury and repair. J Anat 2003, 203, (1), 89–99. [PubMed: 12892408]
2. Mauro A, Satellite cell of skeletal muscle fibers. J Biophys Biochem Cytol 1961, 9, 493–5. [PubMed: 13768451]
3. Terada N; Takayama S; Yamada H; Seki T, Muscle repair after a transsection injury with development of a gap: an experimental study in rats. Scand J Plast Reconstr Surg Hand Surg 2001, 35, (3), 233–8. [PubMed: 11680391]
4. Badylak SF; Freytes DO; Gilbert TW, Extracellular matrix as a biological scaffold material: Structure and function. Acta Biomater 2009, 5, (1), 1–13. [PubMed: 18938117]
5. Gilbert TW; Sellaro TL; Badylak SF, Decellularization of tissues and organs. Biomaterials 2006, 27, (19), 3675–83. [PubMed: 16519932]
6. Merritt EK; Cannon MV; Hammers DW; Le LN; Gokhale R; Sarathy A; Song TJ; Tierney MT; Suggs LJ; Walters TJ; Farrar RP, Repair of traumatic skeletal muscle injury with bone-marrow-derived mesenchymal stem cells seeded on extracellular matrix. Tissue Eng Part A 2010, 16, (9), 2871–81. [PubMed: 20412030]

7. Ott HC; Matthiesen TS; Goh SK; Black LD; Kren SM; Netoff TI; Taylor DA, Perfusion-decellularized matrix: using nature's platform to engineer a bioartificial heart. Nat Med 2008, 14, (2), 213–21. [PubMed: 18193059]
8. Uygun BE; Soto-Gutierrez A; Yagi H; Izamis ML; Guzzardi MA; Shulman C; Milwid J; Kobayashi N; Tilles A; Berthiaume F; Hertl M; Nahmias Y; Yarmush ML; Uygun K, Organ reengineering through development of a transplantable recellularized liver graft using decellularized liver matrix. Nat Med 2010, 16, (7), 814–20. [PubMed: 20543851]
9. Ott HC; Clippinger B; Conrad C; Schuetz C; Pomerantseva I; Ikonomou L; Kotton D; Vacanti JP, Regeneration and orthotopic transplantation of a bioartificial lung. Nat Med 2010, 16, (8), 927–33. [PubMed: 20628374]
10. Sullivan DC; Mirmalek-Sani SH; Deegan DB; Baptista PM; Aboushwareb T; Atala A; Yoo JJ, Decellularization methods of porcine kidneys for whole organ engineering using a high-throughput system. Biomaterials 2012, 33, (31), 7756–64. [PubMed: 22841923]
11. Jank BJ; Xiong L; Moser PT; Guyette JP; Ren X; Cetrulo CL; Leonard DA; Fernandez L; Fagan SP; Ott HC, Engineered composite tissue as a bioartificial limb graft. Biomaterials 2015, 61, 246–56. [PubMed: 26004237]
12. Merritt EK; Hammers DW; Tierney M; Suggs LJ; Walters TJ; Farrar RP, Functional assessment of skeletal muscle regeneration utilizing homologous extracellular matrix as scaffolding. Tissue Eng Part A 2010, 16, (4), 1395–405. [PubMed: 19929169]
13. Mirsadraee S; Wilcox HE; Korossis SA; Kearney JN; Watterson KG; Fisher J; Ingham E, Development and characterization of an acellular human pericardial matrix for tissue engineering. Tissue Eng 2006, 12, (4), 763–73. [PubMed: 16674290]
14. Barbosa I; Garcia S; Barbier-Chassefiere V; Caruelle JP; Martelly I; Papy-Garcia D, Improved and simple micro assay for sulfated glycosaminoglycans quantification in biological extracts and its use in skin and muscle tissue studies. Glycobiology 2003, 13, (9), 647–53. [PubMed: 12773478]
15. Edwards CA; O'Brien WD, Jr., Modified assay for determination of hydroxyproline in a tissue hydrolyzate. Clinica chimica acta; international journal of clinical chemistry 1980, 104, (2), 161–7. [PubMed: 7389130]
16. Lasher RA; Wolchok JC; Parikh MK; Kennedy JP; Hitchcock RW, Design and characterization of a modified T-flask bioreactor for continuous monitoring of engineered tissue stiffness. Biotechnol Prog 2010, 26, (3), 857–64. [PubMed: 20187075]
17. Wolchok JC; Brokopp C; Underwood CJ; Tresco PA, The effect of bioreactor induced vibrational stimulation on extracellular matrix production from human derived fibroblasts. Biomaterials 2009, 30, (3), 327–35. [PubMed: 18937972]
18. Wolchok JC; Tresco PA, The isolation of cell derived extracellular matrix constructs using sacrificial open-cell foams. Biomaterials 2010.
19. Huang NF; Lee RJ; Li S, Engineering of aligned skeletal muscle by micropatterning. Am J Transl Res 2010, 2, (1), 43–55. [PubMed: 20182581]
20. Liu B; Qu MJ; Qin KR; Li H; Li ZK; Shen BR; Jiang ZL, Role of cyclic strain frequency in regulating the alignment of vascular smooth muscle cells in vitro. Biophys J 2008, 94, (4), 1497–507. [PubMed: 17993501]
21. Crapo PM; Gilbert TW; Badylak SF, An overview of tissue and whole organ decellularization processes. Biomaterials 2011, 32, (12), 3233–43. [PubMed: 21296410]
22. Zhang Y; He Y; Bharadwaj S; Hammam N; Carnagey K; Myers R; Atala A; Van Dyke M, Tissue-specific extracellular matrix coatings for the promotion of cell proliferation and maintenance of cell phenotype. Biomaterials 2009, 30, (23–24), 4021–8. [PubMed: 19410290]
23. Lee KI; Lee JS; Kim JG; Kang KT; Jang JW; Shim YB; Moon SH, Mechanical properties of decellularized tendon cultured by cyclic straining bioreactor. J Biomed Mater Res A 2013, 101, (11), 3152–8. [PubMed: 23554286]
24. Harrison RD; Gratzer PF, Effect of extraction protocols and epidermal growth factor on the cellular repopulation of decellularized anterior cruciate ligament allografts. J Biomed Mater Res A 2005, 75, (4), 841–54. [PubMed: 16123978]

25. Sutherland AJ; Beck EC; Dennis SC; Converse GL; Hopkins RA; Berkland CJ; Detamore MS, Decellularized cartilage may be a chondroinductive material for osteochondral tissue engineering. PLoS One 2015, 10, (5), e0121966. [PubMed: 25965981]
26. Chen YC; Chen RN; Jhan HJ; Liu DZ; Ho HO; Mao Y; Kohn J; Sheu MT, Development and Characterization of Acellular Extracellular Matrix Scaffolds from Porcine Menisci for Use in Cartilage Tissue Engineering. Tissue Eng Part C Methods 2015.
27. Pasella S; Baralla A; Canu E; Pinna S; Vaupel J; Deiana M; Franceschi C; Baggio G; Zinellu A; Sotgia S; Castaldo G; Carru C; Deiana L, Pre-analytical stability of the plasma proteomes based on the storage temperature. Proteome science 2013, 11, (1), 10. [PubMed: 23518135]
28. Wang J; Zhu HH; Xue JH; Wu SS; Chen Z, Effects of storage conditions on the stability of serum CD163, NGAL, HMGB1 and MIP2. International journal of clinical and experimental pathology 2015, 8, (4), 4099–105. [PubMed: 26097598]
29. Cebotari S; Tudorache I; Jaekel T; Hilfiker A; Dorfman S; Ternes W; Haverich A; Lichtenberg A, Detergent decellularization of heart valves for tissue engineering: toxicological effects of residual detergents on human endothelial cells. Artif Organs 2010, 34, (3), 206–10. [PubMed: 20447045]
30. Faulk DM; Carruthers CA; Warner HJ; Kramer CR; Reing JE; Zhang L; D'Amore A; Badylak SF, The effect of detergents on the basement membrane complex of a biologic scaffold material. Acta Biomater 2014, 10, (1), 183–93. [PubMed: 24055455]
31. Greco KV; Francis L; Somasundaram M; Greco G; English NR; Roether JA; Boccaccini AR; Sibbons P; Ansari T, Characterisation of porcine dermis scaffolds decellularised using a novel non-enzymatic method for biomedical applications. Journal of biomaterials applications 2015, 30, (2), 239–53. [PubMed: 25855682]
32. Xing Q; Yates K; Tahtinen M; Shearier E; Qian Z; Zhao F, Decellularization of fibroblast cell sheets for natural extracellular matrix scaffold preparation. Tissue Eng Part C Methods 2015, 21, (1), 77–87. [PubMed: 24866751]
33. Corona BT; Ward CL; Baker HB; Walters TJ; Christ GJ, Implantation of in vitro tissue engineered muscle repair constructs and bladder acellular matrices partially restore in vivo skeletal muscle function in a rat model of volumetric muscle loss injury. Tissue Eng Part A 2014, 20, (3–4), 705–15. [PubMed: 24066899]
34. Kennedy JP; McCandless SP; Rauf A; Williams LM; Hillam J; Hitchcock RW, Engineered channels enhance cellular density in perfused scaffolds. Acta Biomater 2011, 7, (11), 3896–904. [PubMed: 21745609]
35. Montarras D; Morgan J; Collins C; Relaix F; Zaffran S; Cumano A; Partridge T; Buckingham M, Direct isolation of satellite cells for skeletal muscle regeneration. Science 2005, 309, (5743), 2064–7. [PubMed: 16141372]
36. Dahms SE; Piechota HJ; Dahiya R; Lue TF; Tanagho EA, Composition and biomechanical properties of the bladder acellular matrix graft: comparative analysis in rat, pig and human. British journal of urology 1998, 82, (3), 411–9. [PubMed: 9772881]
37. Tottey S; Johnson SA; Crapo PM; Reing JE; Zhang L; Jiang H; Medberry CJ; Reines B; Badylak SF, The effect of source animal age upon extracellular matrix scaffold properties. Biomaterials 2011, 32, (1), 128–36. [PubMed: 20870285]
38. Wang L; Johnson JA; Chang DW; Zhang Q, Decellularized musculofascial extracellular matrix for tissue engineering. Biomaterials 2013, 34, (11), 2641–54. [PubMed: 23347834]
39. Morrissey JB; Cheng RY; Davoudi S; Gilbert PM, Biomechanical Origins of Muscle Stem Cell Signal Transduction. Journal of molecular biology 2015.
40. Rao N; Grover GN; Vincent LG; Evans SC; Choi YS; Spencer KH; Hui EE; Engler AJ; Christman KL, A co-culture device with a tunable stiffness to understand combinatorial cell-cell and cell-matrix interactions. Integrative biology : quantitative biosciences from nano to macro 2013, 5, (11), 1344–54. [PubMed: 24061208]
41. Ribeiro AJ; Ang YS; Fu JD; Rivas RN; Mohamed TM; Higgs GC; Srivastava D; Pruitt BL, Contractility of single cardiomyocytes differentiated from pluripotent stem cells depends on physiological shape and substrate stiffness. Proceedings of the National Academy of Sciences of the United States of America 2015, 112, (41), 12705–10. [PubMed: 26417073]

42. Egusa H; Kobayashi M; Matsumoto T; Sasaki J; Uraguchi S; Yatani H, Application of cyclic strain for accelerated skeletal myogenic differentiation of mouse bone marrow-derived mesenchymal stromal cells with cell alignment. Tissue Eng Part A 2013, 19, (5–6), 770–82. [PubMed: 23072369]

43. Heher P; Maleiner B; Pruller J; Teuschl AH; Kollmitzer J; Monforte X; Wolbank S; Redl H; Runzler D; Fuchs C, A novel bioreactor for the generation of highly aligned 3D skeletal muscle-like constructs through orientation of fibrin via application of static strain. Acta Biomater 2015, 24, 251–65. [PubMed: 26141153]

44. Garvey SM; Russ DW; Skelding MB; Dugle JE; Edens NK, Molecular and metabolomic effects of voluntary running wheel activity on skeletal muscle in late middle-aged rats. Physiological reports 2015, 3, (2).

45. Aurora A; Garg K; Corona BT; Walters TJ, Physical rehabilitation improves muscle function following volumetric muscle loss injury. BMC sports science, medicine and rehabilitation 2014, 6, (1), 41.

46. Wu X; Corona BT; Chen X; Walters TJ, A Standardized Rat Model of Volumetric Muscle Loss for the Development of Tissue Engineering Therapies. BioResearch Open Access 2012, 1, (6).

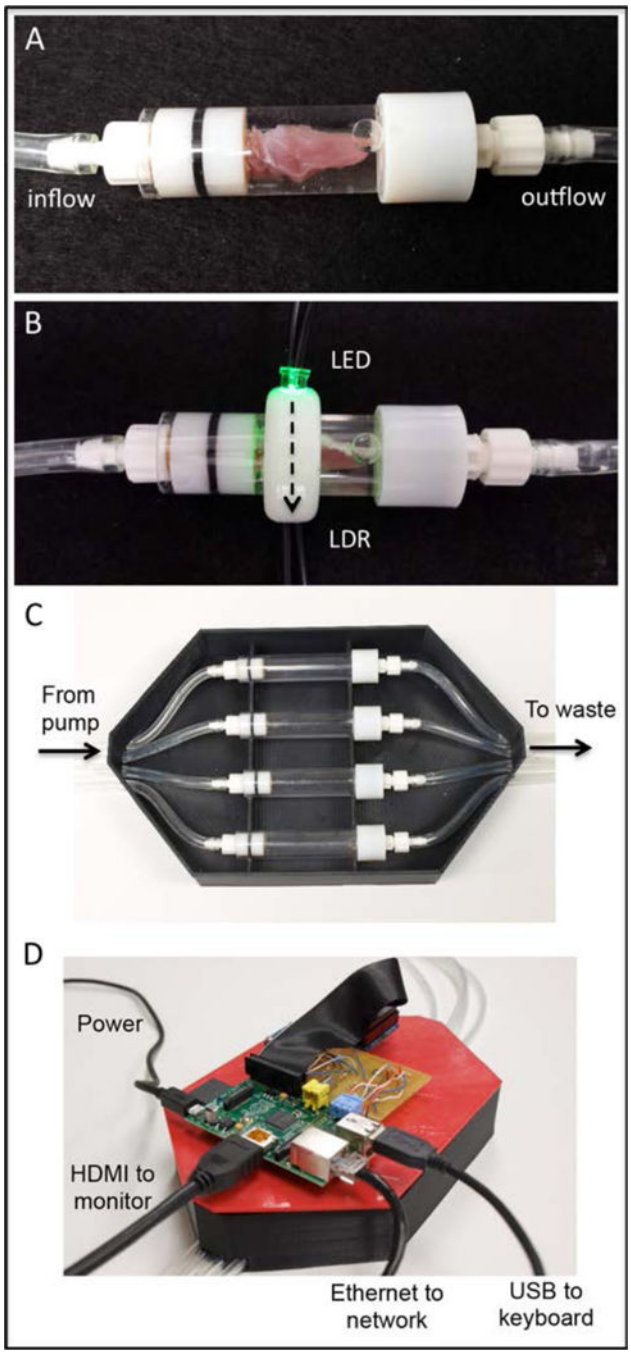

Figure 1:

The primary components of the as built device are the muscle infusion chambers and optical detection collars (A and B). SDS solution is delivered into muscle tissue via a hypodermic needle (not seen), infused through the muscle, and outflows to waste collection. Light produced by the LED travels across the chamber and though the muscle sample (B: dashed arrow) where it is detected and converted to a voltage output by the LDR. Infusion units, optical monitoring collars, and data collection hardware are housed within and mounted onto a custom fabricated enclosure (C and D). The enclosure was designed to accommodate four

side-by-side decellularization units each capable of accommodating a single muscle tissue sample. LDR output voltage was converted to a digital signal (8-bit) and stored with the aid of integrated data collection hardware (Raspberry Pi) and software (Python).

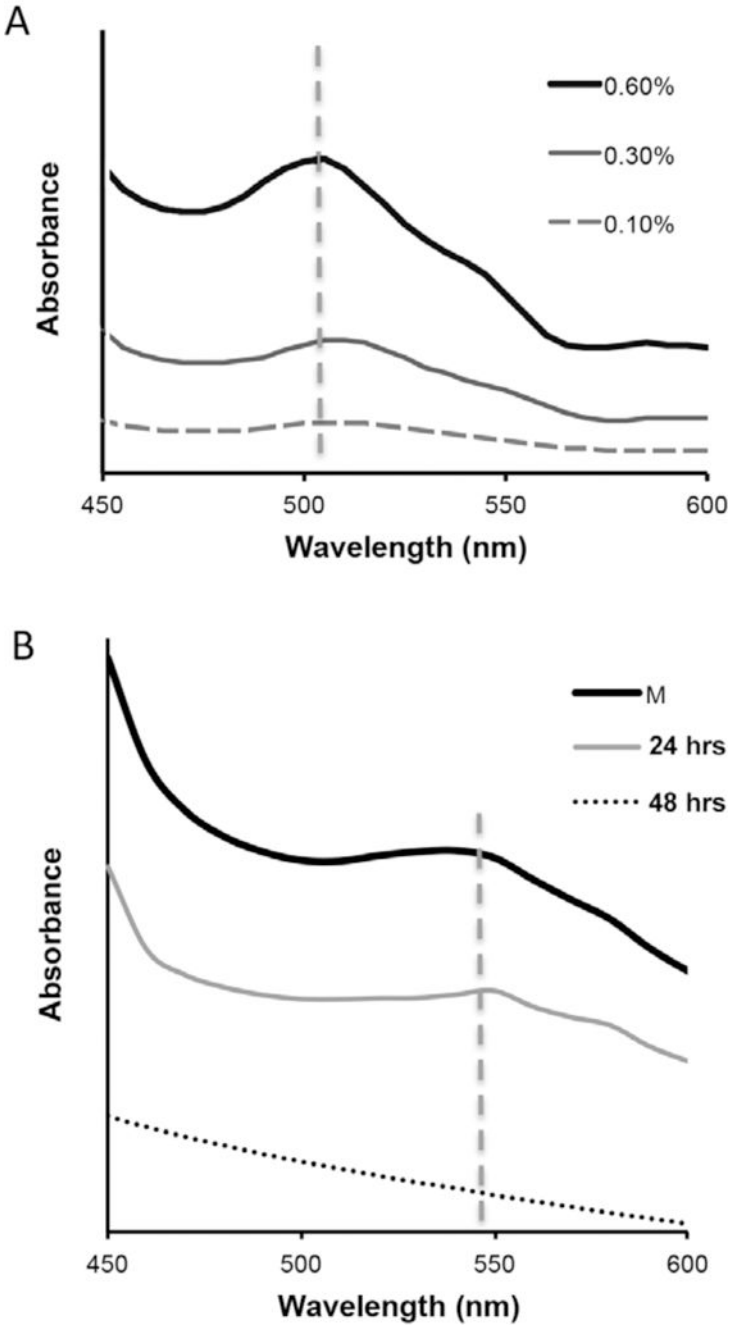

Figure 2:

Representative visible light absorbance spectra for myoglobin solutions (A) and skeletal muscle tissue samples (B). The myoglobin absorbance peak (505±4nm) decreased as protein concentration was diluted from a high of 0.6% (in PBS) to a low of 0.1%. A less pronounced absorbance shoulder (541±7nm) was observed for whole muscle tissue samples. The absorbance shoulder for whole muscle samples (M) was similarly reduced as muscle samples were incubated in decellularization solution (1% SDS) for either 24 or 48 hours.

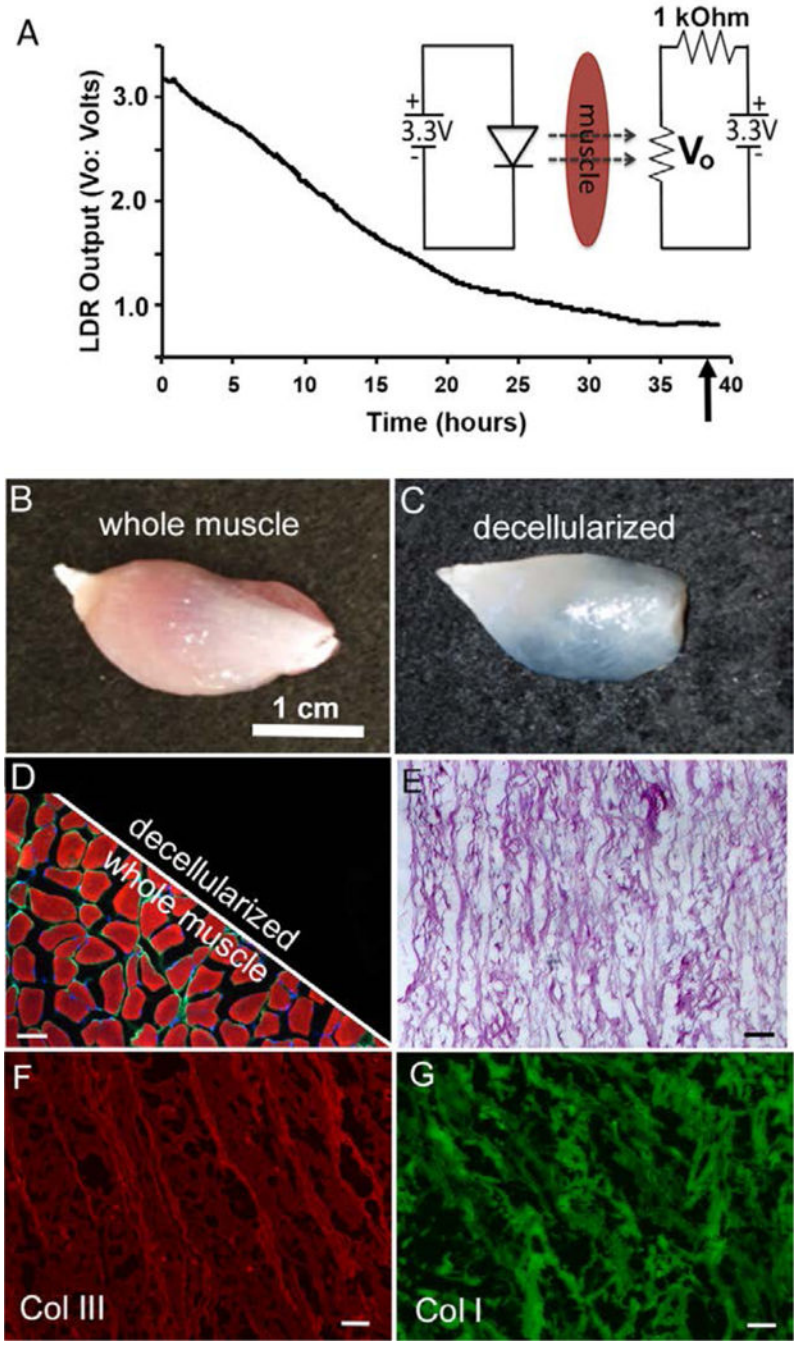

Figure 3:

Representative LDR voltage output (V_o) collected during whole muscle infusion treatment (A). The change in muscle color that occurs during infusion (removal of myoglobin) permitted increased transmission of LED light (535nm) through the tissue, decreasing LDR resistance (A:inset). Decreased LDR resistance was measured and recorded as a change in output voltage (Vo). Prior to infusion, whole muscle tissue samples (B) were strongly reactive (D: left split) to antibodies/molecules directed against actin (red) myoglobin (green) and nuclei (blue). Following infusion treatment (C), recorded as the time to reach a stable

output voltage minimum (A: arrow), actin, myoglobin and nuclei could not be detected in any of the samples tested (D: right split). Infusion prepared DSM samples retained the highly aligned structure of native muscle ECM (E) and were strongly immunoreactive to antibodies directed again collagen I and III (F & G). Unless noted, scale bar = 100um

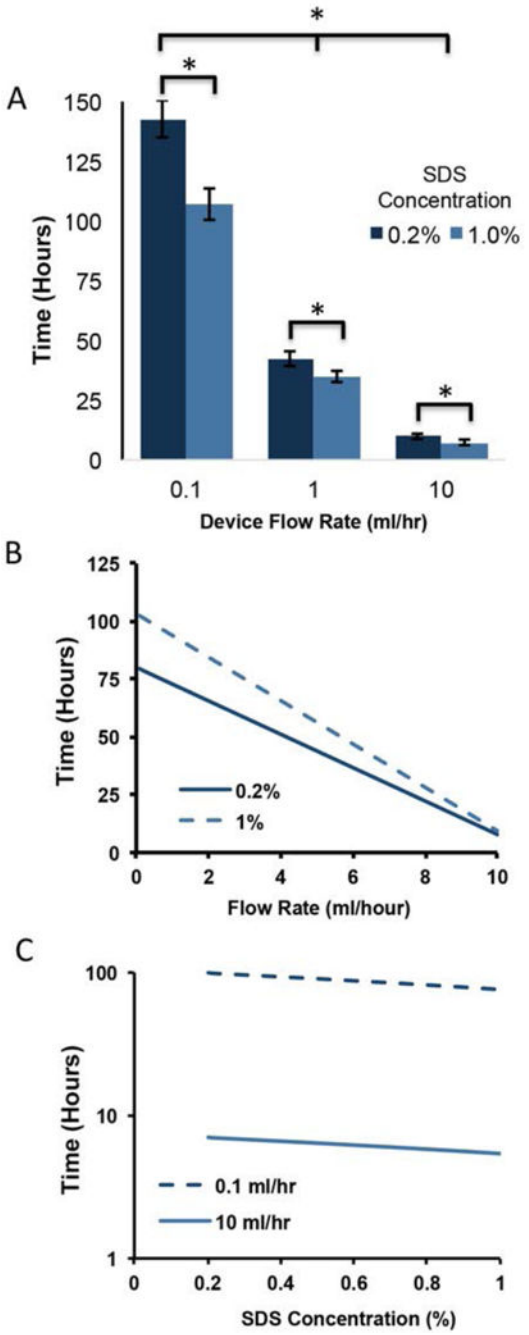

Figure 4:

Both infusion flow rate (ml/hr) and SDS concentration (%) had a significant effect on removal of intracellular myoglobin (A). Values shown are mean+sd. Increases in both flow rate and SDS concentration significantly reduced the time needed to remove myoglobin. * = $p<0.05$; two factor ANOVA. The measured effects of flow (B) and concentration (C) were described using a linear model (see equation 2). Interaction effects between flow and concentration were not observed with the model or detected with ANOVA analysis.

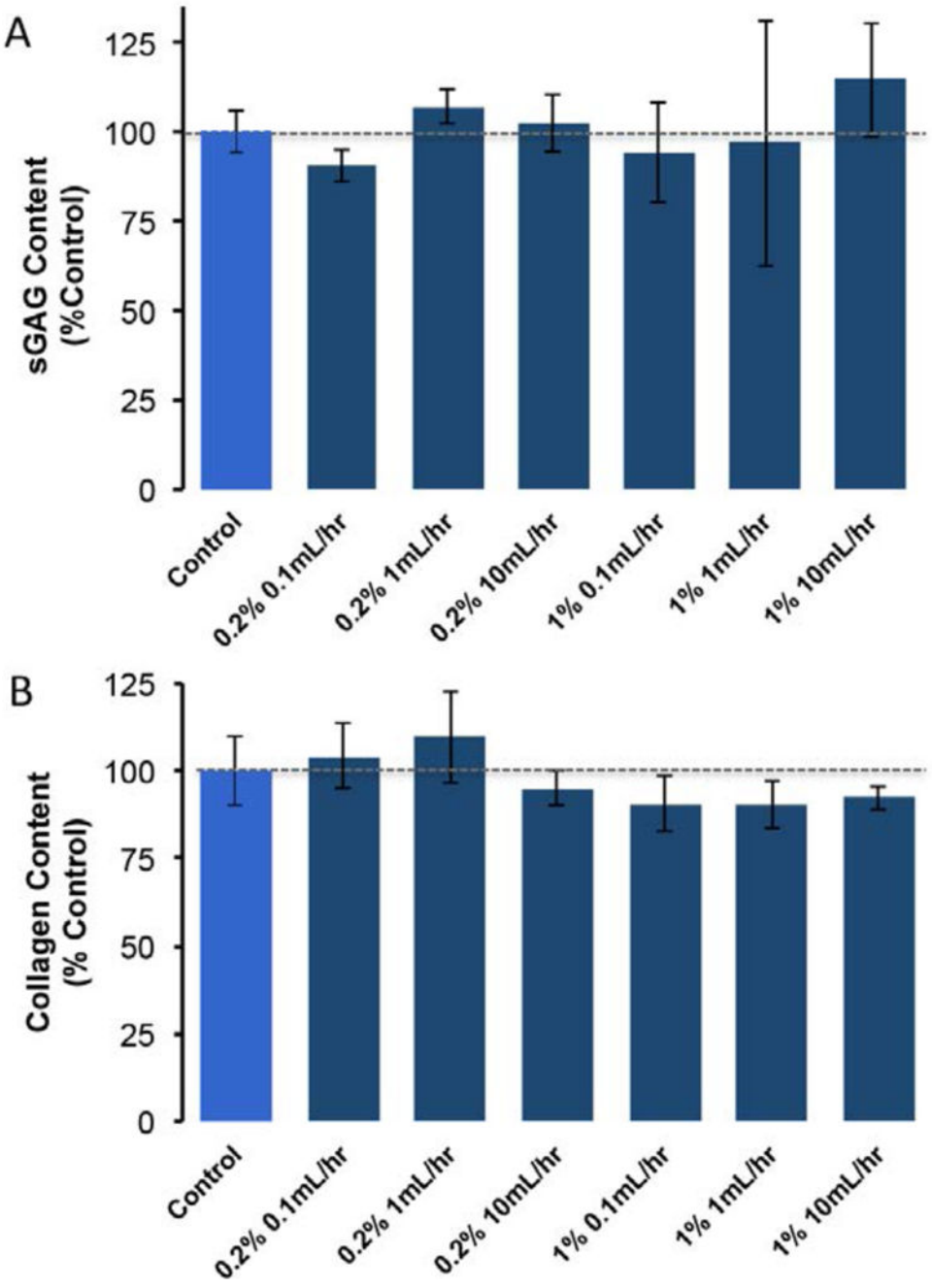

Figure 5:

Infusion treatment did not significantly decrease the collagen or sGAG concentration of DSM samples when compared to non-infused controls. Values shown are mean+sd. $p<0.05$, two factor (flow and concentration) ANOVA.

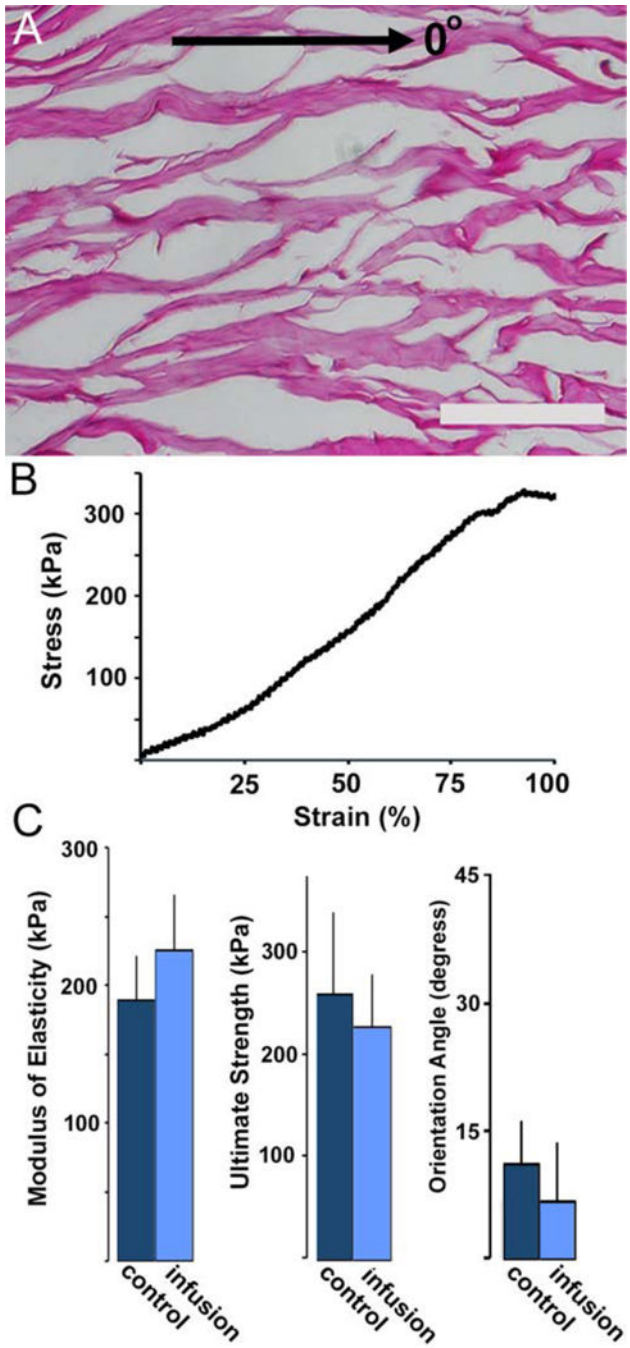

Figure 6:

H&E stained longitudinal (A) sections prepared from infusion DSM samples (0° = direction of muscle contraction). Representative infusion prepared DSM sample stress versus strain curve (B). When compared to controls, infusion treatment did not significantly influence (t-test P>0.05) DSM sample modulus, ultimate strength or alignment values (C). Values shown are mean+sd. Scale bar = 100um.

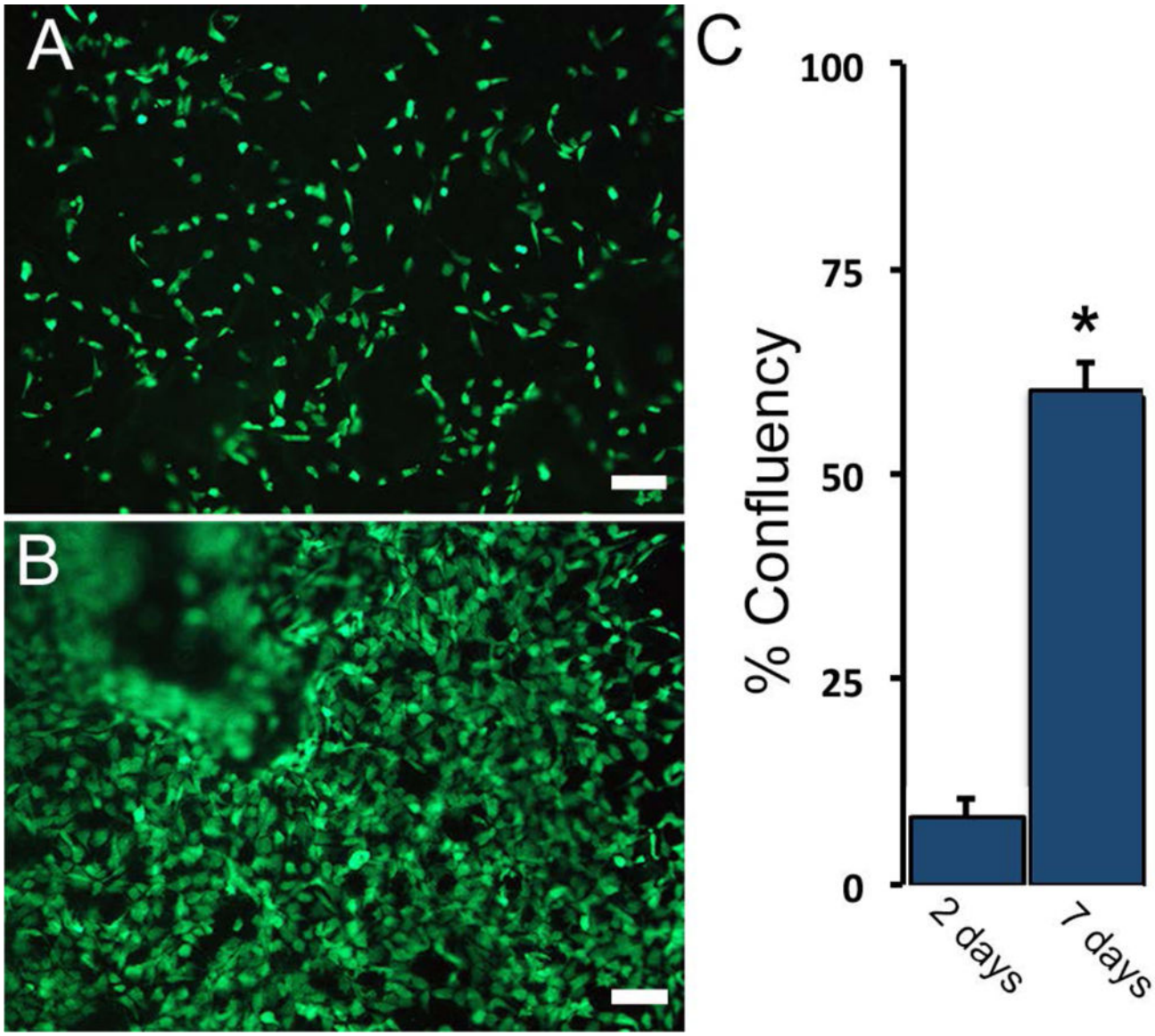

Figure 7:

DSM material substrates supported the in-vitro attachment and proliferation (A and B) of viable (calcein AM) myoblast cells. The percent surface coverage (B) was evaluated at 3 and 7 days post cell seeding. Values shown are mean+sd. * $p<0.05$ compared to day 3, n=4/ sample group, Scale bar = 100um

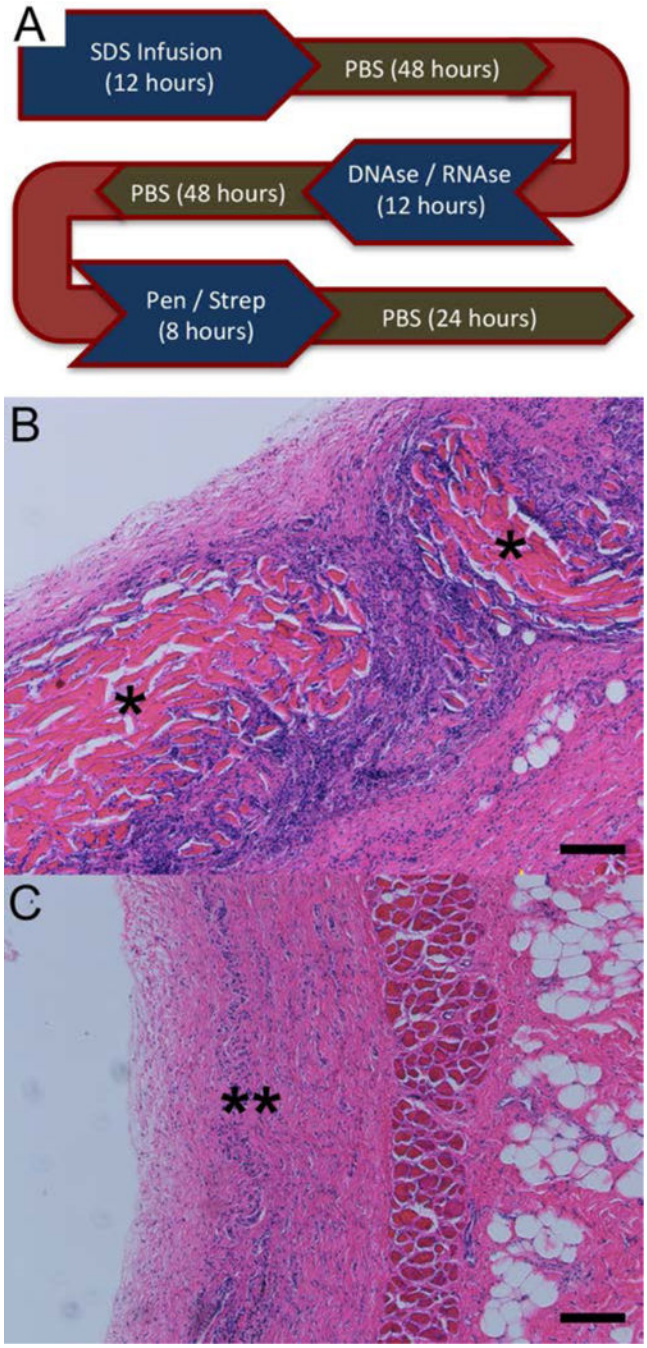

Figure 8:

DSM implants were prepared for implantation using the infusion device to first remove intracellular debris followed by incubation in a DNAse/RNAse solution to remove nuclear debris and penicillin/streptomycin to reduce the risk of implant infection. DSM samples were rinsed in PBS (a total of five 24-hour PBS washes) to remove residual SDS, nuclease, and antibiotic solutions (A). Stained (H&E) tissue sections collected four (B) and twelve weeks (C), following subcutaneous implantation of infusion prepared DSM scaffolds into Sprague Dawley rats. Infusion prepared DSM scaffold fragments were observed within the

dorsal subcutaneous implantation site at 4 weeks (*) but were degraded by 12 weeks (**) in all animals examined (n=3/time point). Scale bar = 100μm